Experimental observations of dual-polarization oscillations in laser-diode-pumped wide-aperture thin-slice Nd:$GdVO_4$ lasers

Jing-Yuan Ko[1], Chi-Ching Lin[2], Kenju Otsuka[3], Yoshihiko Miyasaka[3], Koji Kamikariya[3], Kana Nemoto[4], Ming-Chung Ho[1] and I-Min Jiang[2]

[1]*Department of Physics, National Kaohsiung Normal University, Kaohsiung 824, Taiwan*
[2]*Department of Physics, National Sun Yat-Sen University, Kaohsiung 804, Taiwan*
[3]*Department of Human and Information Science, Tokai University, Kanagawa 259-1292, Japan*
[4]*Department of Physics, Tokai University, Kanagawa 259-1292, Japan*
jyko@nknucc.nknu.edu.tw

Abstract: Dual-polarization oscillations (DPO) on different transitions have been observed for the first time in a mirror-coated thin-slice Nd:$GdVO_4$ laser possessing a large fluorescence anisotropy with laser-diode (LD) pumping. Oscillation spectra, input-output characteristics, pump-dependent pattern formations and noise power spectra are studied experimentally. Simultaneous oscillations of orthogonally-polarized different (higher-order) transverse modes and the resultant violation of inherent antiphase dynamics in multimode lasers have been demonstrated. The experimental results have been explained in terms of the reduced three-dimensional cross-saturation of population inversions among orthogonally-polarized modes peculiar to LD-pumped wide-aperture anisotropic lasers, in which a pumped area is larger than a lasing beam diameter.

OCIS codes: (140.3480) Lasers, diode-pumped; (140.3580) Lasers, solid-state; (260.5430) Polarization; (140.6810) Thermal effects; (190.4420) Nonlinear optics, transverse effects in.

References and links

1. C. He and D. K. Killinger, "Dual-polarization modes and self-heterodyne noise in a single-frequency 2.1-μm microchip Ho,Tm:YAG laser," Opt. Lett. **19,** 396–398 (1994).
2. J. W. Czarske and H. Mueller, "Birefringent Nd:YAG microchip laser used in heterodyne vibrometry," Opt. Commun. **114,** 223–229 (1995).
3. X. J. Wang, S. L. Zhang, G. Liu and L. G. Fei, "Self-Mixing Interference in Dual-Polarization Microchip Nd:YAG Lasers," Chin. Phys. Lett. **21,** 2175–2178 (2004).
4. K. F. Wall and A. Rosiewicz, "Dual-polarization microchip lasers for communications applications," OFC '96 Tech. Dig. paper TuJ1, 50–51 (1996).
5. M. Brunel, A. Amon, and M. Vallet, "Dual-polarization microchip laser at 1.53 μm," Opt. Lett. **30,** 2418–2420 (2005).
6. M. Travagnin, M. P. van Exter, and J. P. Woerdman, "Influence of carrier dynamics on the polarization stability and noise-induced polarization hopping in surface-emitting semiconductor lasers," Phys. Rev. A **56,** 1497–1507 (1997).
7. M. Sciamanna, K. Panajotov, H. Thienpont, I. Veretennicoff, P. Mégret, and M. Blondel, "Optical feedback induces polarization mode hopping in vertical-cavity surface-emitting lasers," Opt. Lett. **28,** 1543–1545 (2003).

#77981 - $15.00 USD Received 11 December 2006; revised 18 January 2007; accepted 25 January 2007

8. B. Nagler, M. Peeters, J. Albert, G. Verschaffelt, K. Panajotov, H. Thienpont, I. Veretennicoff, J. Danckaert, S. Barbay, G. Giacomelli, and F. Marin, "Polarization-mode hopping in single-mode vertical-cavity surface-emitting lasers: Theory and experiment," Phys. Rev. A **68,** 013813 (2003).
9. B. S. Ryvkin, K. Panajotov, E. A. Avrutin, I. Veretennicoff, and H. Thienpont, "Optical-injection-induced polarization switching in polarization-bistable vertical-cavity surface-emitting lasers," J. Appl. Phys. **96,** 6002–6007 (2004).
10. E. Cabrera, S. Melle, O. G. Calderón, and J. M. Guerra, "Evolution of the Correlation between Orthogonal Polarization Patterns in Broad-Area Lasers," Phys. Rev. Lett. **97,** 233902 (2006).
11. K. Otsuka, K. Kubodera, and J. Nakano, "Stabilized Dual-Polarization Oscillation in a $LiNd_{0.5}La_{0.5}P_4O_{12}$ Laser," IEEE J. Quantum Electron. **13,** 398–400 (1997).
12. K. Otsuka, "Oscillation Properties of Anisotropic Lasers," IEEE J. Quantum Electron. **14,** 49–55 (1978).
13. F. G. Anderson, P. L. Summers, H. Weidner, P. Hong and E. E. Peal, "Interpretive crystal-field parameters: Application to Nd^{3+} in $GdVO_4$ and YVO_4," Phys. Rev. B **50,** 14802–14808 (1994).
14. C. L. Tang, H. Statz, and G. deMars, "Spectral Output and Spiking Behavior of Solid-State Lasers," J. Appl. Phys. **34**, 2289–2295 (1963).
15. K. Otsuka, R. Kawai, Y. Asakawa, P. Mandel and E. A. Viktorov, "Simultaneous single-frequency oscillations on different transitions in a laser-diode-pumped $LiNdP_4O_{12}$ laser," Opt. Lett. **23,** 201–203 (1998).
16. Y. Sato, N. Pavel, and T. Taira, "Spectroscopic properties and near quantum-limit laser-oscillation in Nd:$GdVO_4$ single crystal," in *OSA TOPS on Advanced Solid-State Photonics*, vol. 94, Gregory J. Quarles, Ed., (Optical Society of America, Washington, DC), 405-409 (2004).
17. H. Kogelnik and T. Li, "Laser beams and resonators," Proc. IEEE **54,** 1312–1329 (1966).
18. T. Kimura and K. Otsuka, "Thermal Effects of a Continuously Pumped Nd^{3+}:YAG Laser," IEEE J. Quantum Electron. **7,** 403–407 (1971).
19. Y. Asakawa, R. Kawai, K. Ohki, and K. Otsuka, "Laser-Diode-Pumped Microchip $LiNdP_4O_{12}$ Lasers under Different Pump-Beam Focusing Conditions," Jpn. J. Appl. Phys. **38,** L515–L517 (1999).
20. P. Mandel, K. Otsuka, J. Wang, and D. Pieroux, "Two-Mode Laser Power Spectra," Phys. Rev. Lett. **76,** 2694–2697 (1996).
21. P. Mandel, B. A. Nguyen, and K. Otsuka, "Universal dynamical properties of three-mode Fabry-Perot lasers," Quantum Semiclassic. Opt. **9,** 365–380 (1997).
22. K. Otsuka, "Transverse Effects on Antiphase Laser Dynamics," Jpn. J. Appl. Phys. **32,** L1414–L1417 (1993).

1. Introduction

Dual-polarization oscillations (DPO) in LD-pumped microchip solid state lasers are useful for a variety of applications, ranging from heterodyne interferometry [1, 2, 3] to optical communications [4, 5]. DPO has also attracted much attention from the physics point of view, and similar DPO and related phenomena, including polarization mode hopping in vertical cavity semiconductor lasers (VCSELs) [6, 7, 8, 9]; dynamic pattern formations in pulsed solid-state lasers [10], have been reported. DPO can be implemented in isotropic lasers whose birefringence results from residual stress [1], mechanical stress [3], or a composite birefringent element [5], even though laser emissions are unpolarized in isotropic laser materials, such as Nd:YAG, Nd:glass, Er, Yb:glass etc.

Otsuka et. al. [11] observed DPO in a $LiNd_{0.5}La_{0.5}P_4O_{12}$ laser possessing a fluorescence anisotropy and suggested that the laser can oscillate in DPO because emission cross sections along the indicatrix axes are close to each other, i.e., the emission cross-section ratio, R, is less than 2 [12]. While, the standard mode-matched LD-pumped solid-state lasers possess larger fluorescence anisotropies (e.g., Nd:$GdVO_4$), whose lasing mode profile (i.e., TEM_{00}) being restricted by the external cavity is matched to the pump beam profile, the strong cross-saturation of population inversions among modes through longitudinal spatial hole-burning prevents DPO due to the large difference in emission cross sections.

This paper reports experimental observations of DPO in a LD-pumped wide-aperture thin-slice anisotropic Nd:$GdVO_4$ laser with coated reflective ends for the first time. Oscillation spectra, input-output characteristics, pump-dependent pattern formations and noise power spectra are investigated. It is shown that the wide-aperture laser configuration with a large pumped area makes DPO possible in Nd:$GdVO_4$ with a large fluorescence anisotropy, i.e., $R \simeq 5$, featuring

#77981 - $15.00 USD Received 11 December 2006; revised 18 January 2007; accepted 25 January 2007

simultaneous oscillations of different (higher-order) transverse modes for orthogonal-polarized emissions. The resultant violation of inherent antiphase dynamics in multimode lasers have been demonstrated and explained in terms of the reduced three-dimensional cross-saturation of population inversions among orthogonally-polarized modes peculiar to LD-pumped wide-aperture anisotropic lasers, in which the pumped area is larger than the lasing beam diameter.

2. Experimental apparatus

The experimental setup for a LD pumped microchip laser is shown in Fig. 1. A 5-mm square, *a*-cut, 3%-doped Nd:$GdVO_4$ (CASTECH Inc.) laser crystal with 1-mm-thick plane parallel Fabry-Perot resonator was used. One end-surface of the crystal was coated to be transmissive (95%) at the LD pump wavelength of 808 nm and highly reflective (99.8%) at the lasing wavelength of 1063 nm. The other surface was coated to be 99% reflective at 1063 nm and < 5 % reflective at 808 nm. The polarization of the LD pump beam is parallel to the *c*-axis of the laser crystal. A collimated elliptical-shaped LD pump beam was passed through an anamophic prism pair to transform the beam shape to the circular one and focused on the crystal by a microscope objective lens (magnification, $10\times$; numerical aperture, 0.25).

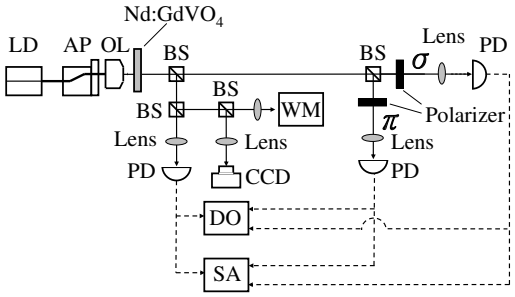

Fig. 1. Experimental setup of a LD-pumped wide aperture thin-slice Nd:$GdVO_4$ laser. LD: laser diode, AP: anamorphic prism pair, OL: objective lens, BS: beam splitter, PD: photodiode receiver, WM: multiwavelength meter, CCD: charge-coupled device, DO: digital oscilloscope, SA: rf spectrum analyzer.

The lasing beam was divided to obtain two beams by a beam splitter. One beam was used for the measurement of the total output. The other beam was split into two beams and individual beams were passed through polarizers to obtain π and σ-polarization modal outputs, respectively. The three beams were detected by InGaAs photoreceivers (New Focus 1811, 125-MHz bandwidth) followed by a digit oscilloscope (Tektronix TDS5054, 500-MHz bandwidth, 5Gs/s sampling period) and a spectrum analyzer (Advantest R3132, frequency range: 9kHz-3GHz).

3. Experimental results

3.1. Oscillation spectra and input-output characteristics

Global oscillation spectra were measured by a multiwavelength meter (Agilent 86142B: wavelength range 600 nm - 1700 nm). The pump power dependence of the oscillating spectrum is shown in Fig. 2 (a), where modes 1 and 1' are adjacent longitudinal modes belonging to the ${}^4F_{3/2}(2) \rightarrow {}^4I_{11/2}(1)$ transition at 1062.92 nm and 1063.22 nm, mode 2 the ${}^4F_{3/2}(1) \rightarrow {}^4I_{11/2}(1)$ transition at 1063.04 nm and mode 3 the ${}^4F_{3/2}(2) \rightarrow {}^4I_{11/2}(2)$ transition at 1065.42 nm, where the longitudinal mode spacing of the 1-mm-thick Nd:$GdVO_4$ laser is

#77981 - $15.00 USD Received 11 December 2006; revised 18 January 2007; accepted 25 January 2007

0.28 nm. The energy level diagram and lasing transitions are depicted in Fig. 2 (b), in which the experimental stark levels were measured by Anderson et. al. [13]. ℓ_1, ℓ_2 and ℓ_3 are the ${}^4F_{3/2}(2) \rightarrow {}^4I_{11/2}(1)$, ${}^4F_{3/2}(1) \rightarrow {}^4I_{11/2}(1)$, and ${}^4F_{3/2}(2) \rightarrow {}^4I_{11/2}(2)$ transitions respectively.

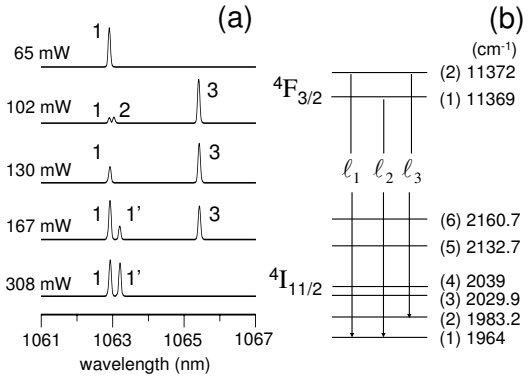

Fig. 2. (a). Global oscillation spectra at several pump levels. The lasing threshold is 62 mW. (b) Stark energy levels (in cm^{-1}) of ${}^4I_{11/2}$ and ${}^4F_{3/2}$ for Nd^{+3} in $GdVO_4$ crystals. ℓ_1 represents the transition for modes 1 and 1', while ℓ_2 and ℓ_2 correspond to the transitions for modes 2 and 3 in (a).

Figure 3 shows the total and modal input-output characteristics. The modal output power was accurately calibrated from the measured total output power and intensity ratios in the global oscillation spectra. The expected increase of total intensity is displayed with the increase of pump power. However, when the pump is increased, modal outputs 2 and 3 tend to decrease, and finally stop lasing. Besides, the modal output powers cross at point C. Although only linear modal outputs are obtained within the framework of the Tang-Statz-deMars model [14] for the multimode lasers, Otsuka et. al. [15] introduced the effect of population-inversion cross saturation to explain the negative slope efficiency and the crossing of modal outputs in a laser-diode-pumped $LiNdP_4O_{12}$ operating in a three-transition regime. Therefore, the negative slope efficiency, indicated by the arrow, and the crossing of modal outputs in the present system may be attributed to the effect of cross-saturation of population inversions among lasing modes on different transitions. The number of oscillating modes are also represented in Fig. 3. When the pump power increases, the different transitions occur in the sequence: (1)→(1,2,3)→(1,3)→(1,1',3).

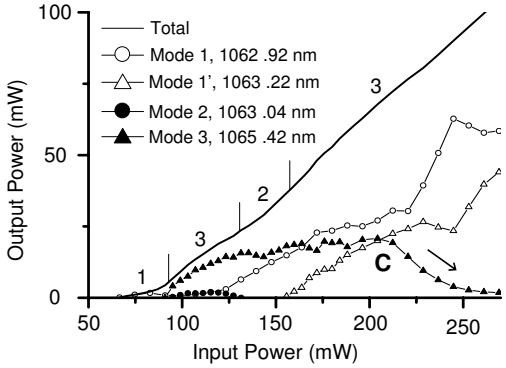

Fig. 3. Input-output characteristics of a LD-pumped wide aperture thin-slice Nd:$GdVO_4$ laser.

#77981 - $15.00 USD Received 11 December 2006; revised 18 January 2007; accepted 25 January 2007

3.2. *Polarizations of lasing modes and pump-dependent pattern formation*

Let us examine the polarization properties of lasing modes belonging to the three transition lines ℓ_1, ℓ_2, and ℓ_3. The total output was passed through a polarizer and measured by a multiwavelength meter. Figure 4 (a) shows the global oscillation spectra for $\theta = 0^\circ$ and $\theta = 90^\circ$, wherein the angle $\theta = 0^\circ$ is defined as the direction of the polarizer parallel to the *c*-axis of the crystal. The results indicate that the polarization direction of mode 1 is parallel to the *c*-axis of the crystal, and those of modes 2 and 3 are perpendicular to the *c*-axis.

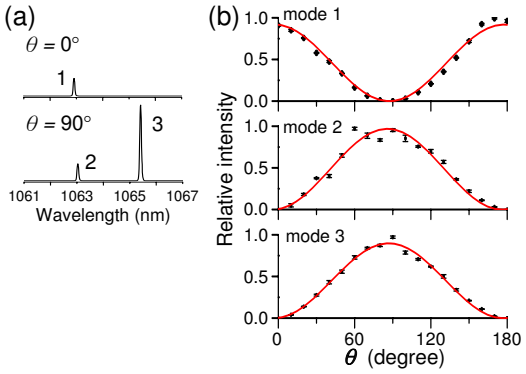

Fig. 4. The LD-pumped wide-aperture thin-slice Nd:$GdVO_4$ laser operating in the three-transition oscillation regime: (a) the global oscillation spectra with the angle of the polarizer parallel ($\theta = 0^\circ$) and perpendicular ($\theta = 90^\circ$) to the *c*-axis of the crystal; (b) the relative intensities of lasing modes as a function of the angle θ of the polarizer to the *c*-axis of the crystal.

The linear polarizations of lasing modes were also confirmed by the relative intensities of lasing modes as a function of the angle θ shown in Fig. 4 (b). Mode 1 is linearly polarized and parallel to *c*-axis of the crystal (π-polarization). On the other hand, modes 2 and 3 are linearly polarized and perpendicular to *c*-axis of the crystal (σ-polarization). In short, a π-polarized emission was produced by the ℓ_1 transition, while σ-polarized emissions were produced by ℓ_2 and ℓ_3 transitions. Hence, the total output includes two orthogonal polarization lasing beams; thus the present LD-pumped wide-aperture microchip Nd:$GdVO_4$ laser exhibits dual polarization oscillations (DPO).

On the contrary, DPO has yet to be attained in standard mode-matched LD-Nd:$GdVO_4$ lasers with external cavity configurations, because the emission cross sections of Nd:$GdVO_4$ for π-polarized emission of 10.3×10^{-19}-cm^2 at 1063-nm is 5 times larger than those of σ-polarized emissions, 2.1×10^{-19}-cm^2, at 1063-nm and 1065-nm [16]. Consequently, DPO obtained in the present experiment is considered to arise from the peculiar nature of LD-pumped thin-slice wide-aperture laser schemes. In industrial applications of dual-polarization oscillations, we suggest that DPO can be obtained even in anisotropic lasers possessing large fluorescence anisotropies like Nd:$GdVO_4$ by controlling the pump-beam focusing condition such that the pump-beam spot size is larger than the lasing-beam spot size determined by the optical resonator, while the linearly-polarized emission takes place under the mode-matched pumping condition.

Next, let us show the unique lasing pattern formations associated with DPO. Figure 5 shows the pump-dependent far-field lasing patterns of π and σ-polarization modes. In the low pump-power region, in which optical confinement due to the thermal lens effect is weak, both π and σ-polarization emissions exhibit TEM_{00}-like profiles, whose intensity distributions peak at

#77981 - $15.00 USD Received 11 December 2006; revised 18 January 2007; accepted 25 January 2007

slightly different positions across the large pumped area as compared with the lasing spot sizes, as shown in Figs. 5 (a)-(b) and (a')-(b'). Therefore, these two lasing modes are considered to be spatially-separated localized modes. As the pump power is increased, the transverse optical confinement is increased due to the increased thermal lens effect and π-polarized emission forms a TEM_{00} mode, while σ-polarization emission tends to form high order Hermit-Gaussian modes, TEM_{10} and TEM_{20} in sequence as shown in Figs. 5 (c)-(d) and (c')-(d').

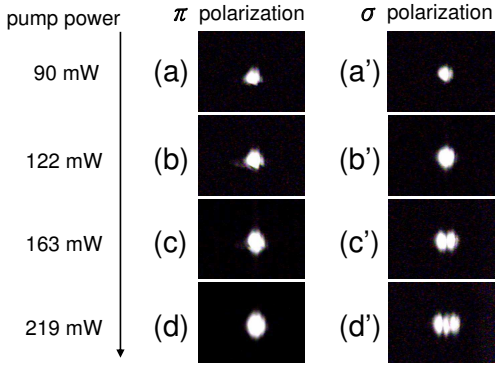

Fig. 5. Far-field lasing pattern changes of π- and σ-polarization modes with increasing pump power. The associated movie file, indicating the pump-dependent far-field lasing patterns, has a size of 1.08 Mbytes for the π-polarization mode and 1.66 Mbytes for the σ-polarization mode, respectively.

The spot sizes at the input and output mirrors, w_1 and w_2, were shown as a function of the effective focal length of the thermal lens, f, in Fig. 6. Here, w_1 and w_2 are given by [17]

$$w_i^2 = \frac{\lambda n_0 L}{\pi g_i}\sqrt{\frac{g_1 g_2}{1-g_1 g_2}} \tag{1}$$

where λ is the wavelength of a laser mode, n_0 = 2.0 is the refractive index of Nd:$GdVO_4$, $L = 1$ mm is the cavity length, $g_1 = 1 - n_0 L/(2f)$, and $g_2 = 1$. The effective focal length of the thermal lens f is estimated by [18, 19]

$$\frac{1}{f} \approx \frac{L_e A}{2K_C}\left[\frac{dn}{dT} + \alpha_E (n_0 - 1)\right]. \tag{2}$$

Here, L_e is the effective thickness of the thermally induced lens, A is the heat generated per unit volume and time, $K_C \approx 11.7$ W/mK is the thermal conductivity, $dn/dT \approx 4.7 \times 10^{-6}$ K^{-1} is the thermal optical coefficient, and $\alpha_E \approx 1.5 \times 10^{-6}$ K^{-1} is the coefficient of thermal expansion. Accordingly, since A increased, the focal length was considered to decrease as the pump power increased and the pump beam spot size decreased. Lasing spot sizes at the crystal measured by the knife-edge method were 50-60 μm.

The pump-beam spot size, averaged over the absorption length, is indicated by a dashed line in Fig. 6. Note that the pump-beam spot size, which was measured to be 70 μm, is larger than the lasing spot size. Schematic views of pump and lasing beams are depicted in the inset of Fig. 6. As a result, higher order Hermit-Gaussian modes of increased spot size could appear in σ polarization by expending population inversions outside the region of the TEM_{00} field because the pump beam spot size is larger than the lasing TEM_{00} spot size as reported in Ref. [12], even if the stimulated emission cross section for σ-polarization emissions at 1063 nm and 1065 nm are 5 times smaller than that for π-polarization emissions at 1063 nm.

#77981 - $15.00 USD Received 11 December 2006; revised 18 January 2007; accepted 25 January 2007

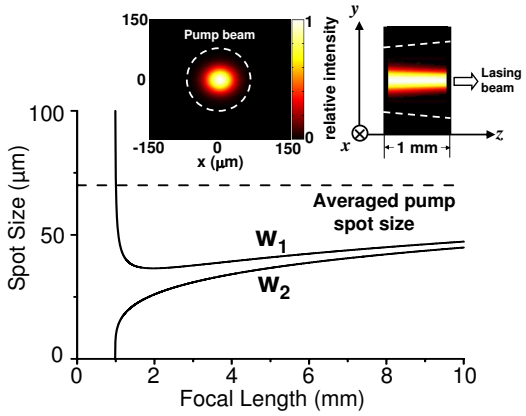

Fig. 6. Calculated lasing beam spot sizes w_1 and w_2 at input and output mirrors as a function of effective focal length. The dashed line indicates the pumping spot size for a microscopic objective lens with $10\times$ magnification. Changes of pump and lasing beams within the laser cavity are depicted in the inset. Left: end view, right: side view.

3.3. Noise power spectra and antiphase dynamics

Finally, let us discuss the three-dimensional cross-saturation effects on antiphase dynamics in DPO operations. Figure 7 (a) shows the global oscillation spectrum at pump power 195 mW for the Nd:$GdVO_4$ laser operating in the two-transition regime. Two adjacent longitudinal modes 1 and 1' on the ℓ_1 transition are π-polarized, while mode 3 on the ℓ_3 transition is σ-polarized. The power spectra of the total, π- and σ-polarization lasing modes are shown in Fig. 7 (b). Figure 7 (c) indicates that the transverse mode pattern of π-polarized emission is TEM_{00} and that of σ-polarized emission is TEM_{10}.

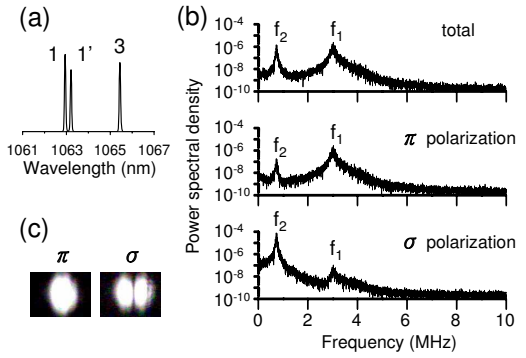

Fig. 7. The Nd:$GdVO_4$ laser operating on a two-transition regime at pump power 195 mW: (a) the global oscillation spectrum; (b) The power spectra of the total, π- and σ-polarization lasing beams; and (c) transverse mode pattern of π- and σ-polarization beams.

The power spectra of modal outputs indicate that each polarization mode shows two different frequency peaks at f_1 and f_2. The power spectral density of the π-polarization mode possesses the strongest noise component at f_1, and that of the σ-polarization mode possesses the strongest noise component at f_2. The lower-frequency relaxation oscillation noise component f_2 appears to reflect cross-saturation dynamics of population inversion among different transverse modes,

#77981 - $15.00 USD Received 11 December 2006; revised 18 January 2007; accepted 25 January 2007

i.e., transverse spatial hole-burning. Contrary to antiphase dynamics due to spatial hole-burning along the longitudinal direction for the same transverse mode, in which lower-frequency relaxation oscillation components cancel each other out for the total output, the lower-frequency component f_2 was not suppressed. The lesser degree of antiphase dynamics may result from the weaker three dimensional cross-saturation between the π- and σ-polarization beams than the usual cross-saturation among longitudinal spatial hole-burning [20, 21]. Note that the noise component, resulting from antiphase dynamics among adjacent modes 1 and 1' that possess the same transverse profile, vanishes for the total output. The power spectra shown in Fig. 7(b) were measured after passing the total and modal beams through optical attenuators to avoid the saturation of the photo-diode and the spectrum analyzer error for higher input voltages than the limitation. Therefore, there is no quantitative relation of vertical scales for modal and total power spectra. However, the degree of antiphase dynamics among orthogonally-polarized emissions can be evaluated correctly from intensity ratios of spectral components at f_1 and lower frequencies in each power spectrum, in which the power spectral density of in-phase components at f_1 for the total is not a simple sum of modal power spectral densities [20]. From this figure, the suppression of the lower frequency relaxation oscillation component at f_2 is found to be small as compared with usual multimode lasers due to the less cross saturation of population inversions among orthogonal modes.

In order to compare the three-dimensional cross-saturation to usual cross-saturation among longitudinal spatial hole-burning, the three-dimensional cross-saturation coefficient β_{ij} is estimated by the ratio of the cross-saturation to self-saturation of the population inversion of the oscillating modes due to "three-dimensional" spatial hole-burning, which is defined as [15, 22]

$$\beta_{ij} = \frac{\int\int\int_{crystal} I_i(x,y,z) I_j(x,y,z) \exp(-\alpha'_p z) dxdydz}{\int\int\int_{crystal} I_i(x,y,z) I_j(x,y,z) \exp(-\alpha'_p z) dxdydz} \tag{3}$$

where the subscript i, j indicates modes, 1, 1', and 3; $\exp(-\alpha'_p z)$ is the exponential spatial distribution of the population inversion; $\alpha'_p = \alpha_p \ell = 7.4$ cm^{-1} is the absorption coefficient normalized by the cavity length ℓ; $I_i(x,y,x)$ and $I_j(x,y,z)$ are the intensity distributions of mode i and j. Here, the modal intensity distributions in rectangular coordinates are given by

$$I_1(x,y,z) = \exp\left[-\frac{2(x^2+y^2)}{w^2(z)}\right] \sin^2(k_1 z) \tag{4}$$

$$I_{1'}(x,y,z) = \exp\left[-\frac{2(x^2+y^2)}{w^2(z)}\right] \sin^2(k_{1'} z) \tag{5}$$

$$I_3(x,y,z) = 8\frac{x^2}{w^2(z)} \exp\left[-\frac{2(x^2+y^2)}{w^2(z)}\right] \sin^2(k_3 z) \tag{6}$$

where $w^2(z) = w_0^2(1+z^2/z_0^2)$ is the beam waist as a function of distance z, $w_0^2 = \lambda z_0/(n_0\pi)$ is the minimum beam waist, $z_0 = [L(2f-L)]^{1/2}$ is the location of the minimum beam waist, L is the cavity length, n_0 is the index of refraction, λ is the lasing wavelength, and f is the thermal focal length; k_1, $k_{1'}$ and k_3 are the longitudinal wavenumbers of modes 1, 1', and 3. We assumed that $w(z)$ can be approximated to be the lasing beam spot size 40 μm, which keeps a constant along the z-axis in the crystal. x and y are normalized by the lasing beam spot size, and z is normalized by the cavity length. $\beta_{11'} \approx 0.849$ is equivalent to the usual longitudinal cross saturation because their transverse patterns are coincident. Therefore, only the highest frequency component f_1 is considered to survive because of the strong cross saturation between adjacent longitudinal modes 1 and 1' having the same transverse profile, as shown in Fig. 7. However, β_{13} and $\beta_{1'3}$ are evaluated to be 8.6×10^{-4} and 8.8×10^{-4}, which are much smaller than $\beta_{11'}$. As a result, the weak cross-saturation coefficient between π and σ-polarization results in a low degree of

#77981 - $15.00 USD Received 11 December 2006; revised 18 January 2007; accepted 25 January 2007

antiphase dynamics and the low-frequency noise component f_2 does not vanish for the total output, as demonstrated in Fig. 7.

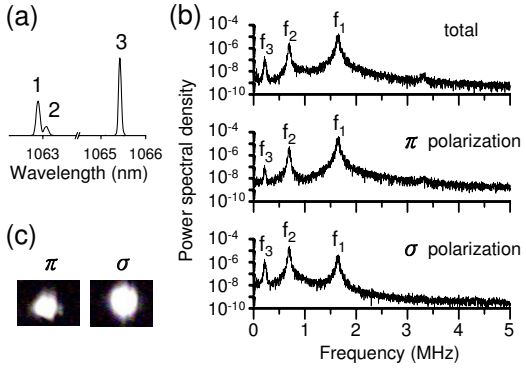

Fig. 8. The Nd:$GdVO_4$ laser was pumped to a three-transition regime by pump power 106 mW: (a) the global oscillation spectrum; (b) The power spectra of the total, π- and σ-polarization lasing beams; and (c) transverse mode pattern of π- and σ-polarization beams. Movie (436 Kbytes) demonstrates the different sizes and positions of the transverse patterns, when the angle of the polarizer changes from 0° to 180°.

The violation of antiphase dynamic peculiar to orthogonally-polarized oscillations in different transverse modes was also verified in the three-transition regime at pump power 106 mW. The global oscillation spectrum is shown in Fig. 8 (a). Mode 1 on the ℓ_1 transition is π-polarized, while mode 2 and 3, on the ℓ_2 and ℓ_3 transitions are σ-polarized. The power spectra of the total, π- and σ-polarization modes are shown in Fig. 8 (b). The power spectra of modal outputs indicate that each polarization mode possesses three different relaxation oscillation frequency components at f_1, f_2, and f_3. The strongest noise component is found at f_1 in the power spectrum of the π-polarized mode and at f_2 in that of the σ-polarized mode. Similarly, the low-frequency relaxation oscillation noise components in the power spectrum of the total output are not suppressed and two lower-frequency components f_2 and f_3 remain in the power spectrum of the total output. Figure 8(c) shows the transverse pattern of the π- and σ-polarization beams. Both beams possess TEM_{00} profiles but the sizes and positions of the transverse patterns are different. Because the transverse patterns of the π- and σ-polarization beams are not overlapping completely, the three-dimensional cross-saturation coefficients among the modes are estimated to be $\beta_{12} = 0.387$, $\beta_{13} = 0.329$, and $\beta_{23} = 0.528$, which are smaller than the usual longitudinal cross saturation coefficients. The violation of antiphase dynamics observed in the present system parallels the fact that a decreased transverse spatial overlapping of population inversion leads to DPO in Nd:$GdVO_4$ lasers with large anisotropy in the emission cross sections. We have observed similar DPO featuring complicated transverse pattern formations under different pump-beam focusing conditions and in Nd:$GdVO_4$ crystals of different thickness.

4. Conclusion

In summary, dual-polarization oscillations in a LD-pumped wide-aperture microchip Nd:$GdVO_4$ laser have been observed. The negative slope efficiency and the crossing of modal outputs of the input-output characteristics, which are similar to the observations of a LD-pumped multi-transition $LiNdP_4O_{12}$ laser [15], reveal the effect of population inversion cross saturation among lasing modes. The wide-aperture LD pumping causes a poor mode matching between the pump beam and lasing beams so that the high order modes were generated. The

#77981 - $15.00 USD Received 11 December 2006; revised 18 January 2007; accepted 25 January 2007

estimated cross saturation of the three-dimensional spatial hole burning is weaker than that of the usual longitudinal cross saturations. The low frequency components cannot be suppressed in the noise power spectra of the total output and the degree of antiphase dynamics are significantly reduced. As a result, DPO in Nd:$GdVO_4$ lasers with large anisotropy in the emission cross sections was brought about because of the decreased transverse spatial overlapping of the population inversions.

These observations suggest that dual-polarization laser oscillations useful for various practical applications are available using anisotropic lasers, which can usually emit only linearly-polarized emissions, by employing LD-pumped wide-aperture laser cavity configurations. The present study also provides insight into pattern formations in dual-polarization lasers, e.g., VCSELs, through transverse cross-saturation of population inversions.

Acknowledgments

This work was partially supported by the National Science Council, Taiwan, under Project No. NSC 93-2112-M-017-004. J.-Y. Ko would like to thank Dr. T.-S. Lim and Dr. R.-S. Guo for helpful discussions.

#77981 - $15.00 USD Received 11 December 2006; revised 18 January 2007; accepted 25 January 2007